EPJ D
Atomic, Molecular, Optical and Plasma Physics
EPJ.org
your physics journal

Eur. Phys. J. D **59**, 13–21 (2010) DOI: 10.1140/epjd/e2010-00116-6

Soliton lasers stabilized by coupling to a resonant linear system

W.J. Firth and P.V. Paulau

EDP SCIENCES
Società Italiana di Fisica
Springer

Eur. Phys. J. D **59**, 13–21 (2010)
DOI: 10.1140/epjd/e2010-00116-6

THE EUROPEAN PHYSICAL JOURNAL D

Regular Article

Soliton lasers stabilized by coupling to a resonant linear system ⋆

W.J. Firth[1] and P.V. Paulau[2,a]

[1] SUPA and Department of Physics, University of Strathclyde, 107 Rottenrow East, Glasgow, G4 0NG, United Kingdom
[2] IFISC (CSIC-UIB), Campus Universitat Illes Balears, 07122 Palma de Mallorca, Spain

Received 22 December 2009 / Received in final form 16 March 2010
Published online 5 May 2010 –

Abstract. Separation into spectral and nonlinear complex-eigenvalue problems is shown to be an effective and flexible approach to soliton laser models. The simplest such model, a complex Ginzburg-Landau model with cubic nonlinearity, has no stable solitonic solutions. We show that coupling it to a resonant *linear* system is a simple and general route to stabilization, which encompasses several previous instances in both space- and time-domains. Graphical solution in the complex eigenvalue plane provides valuable insight into the similarities and differences of such models, and into the interpretation of related experiments. It can also be used predictively, to guide analysis, numerics and experiment.

1 Introduction

Self-localized structures in driven non-equilibrium systems, loosely termed dissipative solitons, have attracted great interest because of their importance in a wide variety of fields. This interest has stimulated several recent books (see e.g. [1,2]) and review articles (see e.g. [3]), as well as a Focus issue [4] and the present Topical issue. Self-localized structures are particularly interesting in optics, because of potential applications to the all-optical control of light, a major thrust of modern photonics. The achievement, control and understanding of cavity solitons (CS) has shown remarkable progress, see, e.g., [5,6] and chapters 3−6 of [1] and op. cit. Most of these works, however, deal with schemes reliant on driving an optical cavity using a broad-area holding beam of high spatial and temporal coherence [6–9]. The complexity and comparative inflexibility of such systems has led to strong recent interest in *cavity soliton lasers* (CSL). For example, a semiconductor-based vertical-cavity CSL could convert broad-area incoherent excitation into a narrow, coherent, power beam of high quality, or into a controllable number of such beams, providing a new approach to microlasers [10–14].

Given the well-known analogies between diffraction and dispersion, there is also interest and merit in considering CSL in the time domain. Indeed, fibre-based pulsed CSL have been the subject of successful theoretical and experimental research for a number of years, see [15–18] and chapters 7−10 of [1]. As well as cross-fertilization between space- and time-domain CSL, there is wide interest in combining the two, i.e. to achieve a viable CSL whose output is self-confined in both space and time, a "laser bullet" system [19]. We will not deal with such systems here, but we will treat both space- and time-domain CSL models in a unified framework, which may help pave the way to the achievement of laser bullets.

To be useful, a CSL system needs to meet criteria governing properties such as simplicity, stability and robustness. System design to satisfy such criteria is obviously greatly assisted if there is a good intuitive understanding of the underlying operating principles of the CSL. In this paper we present a simple and rather general approach to this problem. We separate the task of finding self-confined dissipative structures into two complex eigenvalue problems, each of which has a *family* of solutions leading to *solution curves* in the complex eigenvalue plane. (We call this the X, Y plane, where $X - iY$ is any complex eigenvalue.) Intersections of these curves then correspond to dissipative soliton solutions of the original problem. Typically, one problem is nonlinear, with spatial/temporal coupling and self-localized solutions: we term it the *soliton problem*, though for more general nonlinear structures one could say *structure problem*. The other problem is linear, relating to the complex frequency response of the laser cavity structure, so we call it the *spectral problem*.

A major advantage of splitting the problem in this way is that one can, by varying a parameter in one or other problem, see how the corresponding curve varies, and hence how to "steer" it so as to create (or destroy) soliton-defining intersections. A second advantage is that the same soliton problem can be mated to different spectral problems, and vice versa. (The parameter variation approach just mentioned is actually a special case of this.) More generally, one can, for example, mate one-, two-, or even three-dimensional (1D, 2D, 3D) soliton problems to the same spectral problem. Perhaps more importantly, having solved one soliton problem, e.g. a 3D (bullet) problem, one can experiment with different cavity structures, aiming to devise one whose spectral curve intersects the soliton

⋆ Invited paper
[a] e-mail: p.v.paulau@gmail.com

curve, and does so in a manner indicating that the corresponding solitons (bullets) are stable and robust.

We should stress that stability issues are, strictly speaking, outside the scope of our approach, because the soliton stability problem is not separable in the same way as the soliton existence problem, whose solutions are given by the intersections of the soliton and spectral curves. Nonetheless, certain inferences about stability (and instability) can be drawn from the geometry of these intersecting curves, which is in fact a further benefit of our approach. Furthermore, the stability problem for the "laser-off" state, a necessary condition for soliton stability, can be formulated, solved, and represented in the same X, Y plane as the soliton and spectral curves. This defines explicit and instructive "no-go" (X, Y) domains, which may be easier to visualize and thus implement than the usual parameter inequality conditions (to which they are, of course, equivalent).

The paper is organized as follows: in the following Section 2 we introduce and discuss the simplest CSL model, namely the complex Ginzburg-Landau equation with cubic nonlinearity (CGL3), which is a dissipative generalization of the nonlinear Schrödinger equation (NLS). We (trivially) separate the CGL3 into spectral and soliton problems, present the family of analytic chirped-sech solutions to the soliton problem, and demonstrate the representation of these CGL3 solitons in the X, Y plane. Their known instability is clear in our formulation, and we discuss two alternative strategies for averting this instability. One can either modify the soliton problem by introducing higher-order nonlinearity (e.g. the cubic-quintic extension, CGL5) or, as we stress, one can modify the spectral problem while retaining the analytically-soluble CGL3 soliton problem.

We develop this theme in Section 3, where we consider a simplified model of a vertical-cavity surface-emitting laser (VCSEL) with frequency-selective feedback (FSF) from a Lorentzian filter. We next recast into our framework an earlier time-domain model, of a fibre amplifier coupled to a fibre with resonant linear loss [17], nicely highlighting interesting similarities and differences between these two models. Finally in this section we similarly recast a recent model of a mode-locked fibre laser [18] which includes higher-order nonlinearity in the form of gain saturation. Because, however, the gain saturation is global (time-integrated), analytic chirped-sech pulse solutions are still available through gain rescaling.

Section 4 develops this saturation theme in the context of VCSEL-FSF models by first considering generalization of the CGL3 soliton to allow both for saturated-gain and for 2D solitons (which can only, though easily, be found numerically). Once found, these soliton curves can be interfaced in the X, Y plane to the previous FSF spectral problem. Importantly, they can also be interfaced to the experimentally-important spectral problem corresponding to FSF with delay, which causes the spectral curve to develop multiple loops corresponding to external cavity modes [20,21]. While our present approach cannot describe the dynamical behavior of multi-mode CS lasers, it clearly demonstrates the coexistence of multiple single-soliton solutions corresponding to different cavity modes, and thus to the noise-induced mode-hopping observed experimentally [10,11,22]. Lastly in Section 4, we address the soliton problem for a laser with saturated absorption (LSA), which was one of the first analyzed in the early 1990s, by Rosanov and co-workers [23]. We predict some new LSA regimes when coupling the LSA soliton problem to a non-trivial spectral problem.

Section 5, finally, is a summary, conclusion, and perspective for future developments of our approach.

2 Cubic Ginzburg-Landau laser model

The simplest model for a CSL is the complex Ginzburg Landau equation with cubic nonlinearity (CGL3) [24], for which analytic chirped-sech solitary wave solutions have been known for many years [25–28]. Here we reiterate the CGL3 problem, recasting it into partner soliton and spectral problems, as a simple and instructive example of the technique which is the theme of the present work.

We formulate the CGL3 equation (in 1D meantime) as

$$(\partial_t + 1)\, E = (d + iD)\partial_{xx} E + \left(g_0 - g_2|E|^2\right) E. \qquad (1)$$

The linear spectral operator $\hat{L} = (\partial_t + 1)$ in (1) describes the cavity. It is considered as a simple, passive and lossy system, the "1" representing the cavity loss, to which the evolution coordinate, here the time t, is scaled. On the right side, the nonlinear operator $\hat{N} = (d + iD)\partial_{xx} + (g_0 - g_2|E|^2)$ has terms describing spatial coupling, linear gain/loss (g_0) and cubically-nonlinear gain-loss (g_2). The latter are complex, in general, and characterize the laser medium. Splitting the linear terms into "cavity" and "medium" parts, is obviously not strictly necessary, but it is convenient for our approach to have a mathematical representation of their physically-distinct natures. This will enable us, below, to consider these two linear contributions separately as we analyze different $\hat{L}, \hat{N}$ pairs corresponding to different CSL systems and scenarios. The spatial operator in (1) has a complex coefficient in which d describes diffusive coupling, and D diffractive. In the time domain, D would describe chromatic dispersion, and d would characterize the effects of finite gain bandwidth.

The essence of our approach is to split the full CGL3 problem (1) into two separate complex-eigenvalue problems:

$$\begin{cases} \hat{L}E(x,t) = LE(x,t), \\ \\ \hat{N}E(x,t) = NE(x,t). \end{cases} \qquad (2)$$

Equality of the complex eigenvalues $L = N = X - iY$ obviously defines a solution of the full problem (1). Because equation (1) is invariant on addition of any complex constant to *both* $\hat{L}$ and $\hat{N}$, the origin of the (X, Y) plane is arbitrary, and can be chosen for convenience. Translation in the X direction corresponds to redistributing linear gain/loss between the spectral and nonlinear problems,

while translation in Y represents a change of reference frequency. For example, the complex gain g_0 can always be made real by a shift of reference frequency, but that would make $\hat{L}$ complex.

Our main interest is the existence of single frequency solutions $E = S(x)e^{-i\Omega t}$, which here trivially yields $L = 1 - i\Omega$, i.e. a family of complex eigenvalues parameterized by Ω. Each such family corresponds to a "spectral curve" in the X, Y plane, in this case the simple vertical straight line $(X = 1, Y = \Omega)$.

On the nonlinear side, we are mainly interested in self-localized solutions, for which we must impose the boundary condition $|E| \to 0$ as $|x| \to \infty$. First, however, it is useful to consider, for comparison, linear waves, defining the stability of the zero solution. Setting $E = 0 + \delta E e^{ikx}$, where δE is small, we can immediately write

$$N = N_l = -(d + iD)k^2 + g_0. \tag{3}$$

Setting $N_l = X - iY$, this corresponds to a half-line, parameterized by k^2, emerging from the point corresponding to g_0, its angle dependent on $(d + iD)$. A *necessary* condition of soliton stability is that the N_l half-line has no intersection with the spectral curve L, since any such intersection would represent an appearance of undamped linear wave, and stability of a soliton requires that its background be stable.

Returning to the soliton problem, again we typically find families of eigenvalues N, each family corresponding to a "soliton curve". For simplicity, we will use L (N) to denote any or all of a single complex eigenvalue, the family of eigenvalues, the corresponding curve in the X, Y plane, or a single point of such a curve.

Each intersection of the soliton curve with the spectral curve represents a single-frequency self-localized solution to (1). Such intersections will normally be at isolated points in the X, Y plane, in line with the fact that dissipative solitons are usually isolated solutions. This is because one must balance gain and loss as well as nonlinearity and (e.g.) dispersion. It may seem wasteful to compute two curves to find a single point, but in compensation they convey much more information than the point does. Furthermore, once found the curves can be used to frame and solve other problems, even in totally different systems, as we will see, whereas a solution point, once found, has limited value beyond itself.

It is well known that (1) has analytic soliton solutions of chirped-sech type, and we can derive the soliton curve N analytically for this case. We set $E(x,t) = S(x)e^{-i\Omega t}$, and use the *ansatz*

$$S(x) = A(\cosh(Kx))^{-1-i\beta}. \tag{4}$$

The parameters $A > 0$, $K > 0$ and the chirp parameter β are real. Substitution into the second member of (2) gives two terms in $\mathrm{sech}^2(Kx)$, which must cancel. This constrains the soliton's parameters and thus its contribution to the space-independent terms. Cancellation of the $\mathrm{sech}^2(Kx)$ terms requires:

$$K^2(d + iD)(2 + i\beta)(1 + i\beta) = g_2 A^2. \tag{5}$$

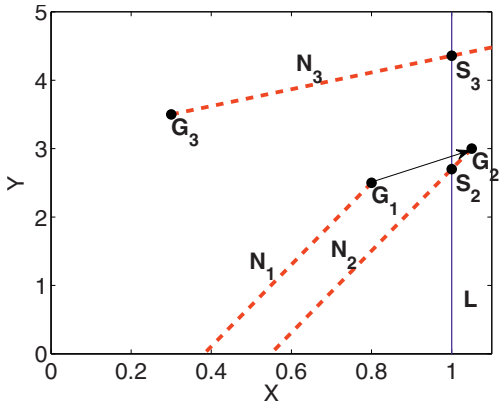

Fig. 1. (Color online) Spectral (L) and soliton (N) lines in the complex eigenvalue plane for the CGL3 (1). When the complex linear gain is at G_1, N_1 and L do not intersect, and there is no soliton solution, but one is created in increasing the gain to G_2 along the arrow. For different parameters, the soliton line N_3 at G_3 may be right-going, giving a soliton at its intersection with L.

This implies, in particular,

$$3\beta K^2 = A^2 \mathrm{Im}\left(g_2/(d + iD)\right). \tag{6}$$

We can extract from (5) a quadratic equation for β which depends only on d, D and g_2. The roots of this equation are real, and their product is -2. Because both A and K are real, (6) determines which root must be chosen. We note, in particular, that the chirp vanishes only when the phase of g_2 matches that of $(d + iD)$, which would be unusual. In that case, the soliton is a simple real sech function, as for the NLS.

Having satisfied (5), the remaining terms yield an expression for the complex eigenvalue N and the soliton curve:

$$N = K^2(d + iD)(1 + i\beta)^2 + g_0 = X - iY. \tag{7}$$

Because β does not depend on K, N is a half-line, parameterized by $K^2 > 0$. It originates in the point $(X = \mathrm{Re}(g_0), Y = -\mathrm{Im}(g_0))$, close to which the solitons have large width (because K is small), and hence small amplitude A, from (6).

Comparing (3) and (7), we note that the half-lines N and N_l are opposed if $\beta = 0$ (as for NLS solitons, which lie "below" the band of linear waves). For finite but small chirp $|\beta| < 1$, they remain largely opposed, which means that it is relatively easy to arrange that N intersects L while N_l does not. If $\beta = \pm 1$ they are orthogonal, while for large chirp, $|\beta| > 1$, N and N_l make an acute angle, and it becomes harder to ensure a stable background for the soliton. In a sense, a highly-chirped sech resembles a linear wave with an amplitude profile more than a true soliton.

Since L is also a straight line for the CGL3 case, N can intersect L at most once (Fig. 1). Intersection requires that $\mathrm{Re}(N) = \mathrm{Re}(L) = 1$, which can usually be achieved by varying $\mathrm{Re}(g_0)$, the linear gain, e.g. from point G_1 to

point G_2 in Figure 1. At G_2, however, the linear gain exceeds the linear loss and the laser-off state is obviously unstable. Therefore so is the corresponding soliton. For different parameters, the soliton line may go to increasing X, e.g. the line N_3 from G_3 in (Fig. 1). The corresponding soliton then has a stable background. It turns out, however, that this soliton is also unstable, due to amplitude instability. Unfortunately, therefore, the CGL3 solitons are always unstable, and so cannot describe any viable CSL.

Now, it is known (see e.g. the paper by Atai and Malomed [17] which we discuss below) that coexistent solutions to nonlinear equations tend to alternate in stability as a function of amplitude. Hence it is no surprise that N_3 also gives rise to an unstable soliton. On the other hand, the same rule suggests that if we can arrange that N and L intersect *twice*, with N emerging from a point with net linear loss, then the second intersection may correspond to a stable soliton (the first being an unstable separatrix). To obtain stable solitons, most authors introduce higher-order nonlinearity. While a laser naturally possesses higher-order nonlinearity in the field E through gain saturation, it typically takes the form $1/(1+|E|^2)$. It turns out that this nonlinearity cannot give stable solitonic pulses or beams because the cubic and quintic nonlinearities are not independent.

Independent control of cubic and quintic nonlinearity in a laser requires the introduction of an additional nonlinear element, such as a saturable absorber [29,30]. This adds several parameters to the model, and significant complication to lasers so based (LSA). We will briefly examine a special case of an LSA model in Section 4. The cubic-quintic (CGL5) model is simplest to allow such control, and its solitonic properties have been extensively studied [1,2] and op. cit. So extensively, indeed, that we will not deal with the CGL5 here, mentioning only that its soliton curve N is a true curve which may, for appropriate parameter choices, intersect the spectral curve twice, even when L is a simple straight line. Hence CGL5 can potentially yield stable laser solitons.

In the next section we examine a different, and in many ways simpler, approach. Instead of stabilizing the soliton through higher-order nonlinearity, we stabilize the background, through frequency-dependent losses. The use of frequency-dependent feedback was recently shown to permit stable two-dimensional (2D) solitons in a vertical-cavity surface emitting laser (VCSEL) [10], and our approach relates to that system. Frequency-dependent loss implies that L will be curved, raising the possibility of a double intersection with N even when the latter is a straight line.

3 Extended CGL3 models

In this section we modify the spectral problem while retaining the analytically-soluble CGL3 soliton problem. We first consider a simplified model of a VCSEL with frequency-selective feedback (FSF) from a Lorentzian filter. We then recast into our framework an earlier time-domain model, of a fibre amplifier coupled to a fibre with

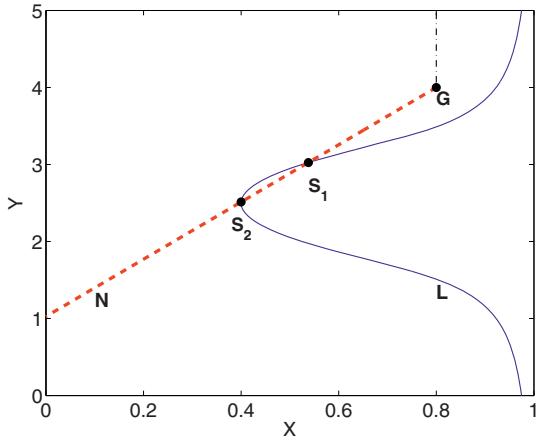

Fig. 2. (Color online) Spectral (L) and soliton (N) lines in the complex eigenvalue plane for the CGL3 with frequency selective feedback (9). When the complex linear gain is at G, N and L intersect twice, so there are two soliton solutions, at S_1 and S_2, with S_2 potentially stable. The vertical line (dash-dotted) relates to linear waves for G. Since it does not intersect L, the soliton background is *stable*.

resonant linear loss [17], and find interesting similarities and differences between these two models. Finally in this section we similarly recast a recent model of a mode-locked fibre laser [18] which includes higher-order nonlinearity in the form of gain saturation. Because, however, the gain saturation is global (time-integrated), analytic chirped-sech pulse solutions are still available through gain rescaling.

We can introduce FSF in a simple and well-behaved way by coupling a second field F to E in $\hat{L}$:

$$\begin{cases} (\partial_t + 1)\, E(x,t) - \sigma^{\frac{1}{2}} F(x,t) = LE(x,t), \\ \partial_t F + (\Gamma_0 + i\Omega_0)\, F = \sigma^{\frac{1}{2}} E. \end{cases} \tag{8}$$

Here σ is a coupling constant, and Ω_0 and Γ_0 are respectively the resonant frequency and linewidth parameter of the field F. Again seeking single-frequency solutions $E = S(x)e^{-i\Omega t}$, $F(x,t) = S_f(x)e^{-i\Omega t}$, we readily obtain

$$L = 1 - i\Omega - \frac{\sigma}{\Gamma_0 + i\,(\Omega_0 - \Omega)}. \tag{9}$$

Clearly this spectral curve asymptotes to the previous vertical line far from resonance, while for $\Omega = \Omega_0$ we have $X = \mathrm{Re}(L) = 1 - \frac{\mathrm{Re}(\sigma)}{\Gamma_0}$. Hence, if $\mathrm{Re}(\sigma)$ is positive the effective cavity loss is reduced for frequencies close to resonance, as in Figure 2. The feedback cannot eliminate the loss completely, or the system would lase without a gain medium, so we require $\sigma < 1$.

In the spatial domain, this spectral behavior can readily be achieved in experiment, with F the field fed back from a grating [10,31] or filter. Dealing first with that case, in the soliton problem we consider pure diffraction ($D = 1, d = 0$), and also slightly modify the our CGL3 gain expression:

$$\hat{N} = i\partial_{xx}E(x,t) + \mu(1 - i\alpha)\left(1 - |E|^2\right)E(x,t). \tag{10}$$

Our problem now corresponds to a greatly-simplified version of a standard VCSEL model [32], modified to describe FSF instead of external injection. Here μ is proportional to the injected current, and thus represents scaled gain in the VCSEL. Evidently $\mu > 0$ if there is gain, while $\mu < 1$ is necessary to prevent lasing of the solitary VCSEL, i.e. to allow a stable off-state. The parameter α, often called the linewidth-enhancement or phase-amplitude-coupling factor, is usually consider to be positive, and moderately large (typically about 5), in VCSELs [3,32].

A major simplification from usual VCSEL models is that we have retained only cubic nonlinearity, which means that this $\hat{N}$ has analytic chirped-sech eigenfunctions, a case not previously considered for VCSEL solitons. Our actual expression can be recognized as the leading terms of an expansion of $\frac{1}{1+|E|^2}$, to which will compare our analytic results in the following section.

As before, the soliton chirp is determined by a quadratic equation involving the parameters, which here takes a particularly simple form:

$$\beta^2 + 3\alpha\beta - 2 = 0. \tag{11}$$

The positive root is required from (6), hence

$$\beta = \frac{3}{2\alpha}\left(\sqrt{1 + 8/9\alpha^2} - 1\right). \tag{12}$$

For $\alpha \gg 1$ we find $\beta \to 2/(3\alpha)$, so that the chirp is already small for $\alpha = 5$. It vanishes for $\alpha \to \infty$, which corresponds to the NLS limit.

Figure 2 shows a situation in which the soliton line from (10) intersects the FSF spectral line from (9) twice, giving two soliton solutions. S_2 is narrower, and has larger amplitude and lower frequency than S_1. In this case the soliton background is stable, because N_l cannot intersect L, and thus there are no undamped linear waves. Of course if the linear gain is changed, such that g_0 lies to the right of L, linear waves, e.g. with $k = 0$, are unstable. Alternatively, if g_0 lies "below" L, then a band of k is unstable (though for this particular model, there are no solitons in that case, because N does not intersect L).

We conclude that our graphical approach readily lends itself to the assessment of the stability of systems to linear waves, noting that in many cases (including the present one) both L and N_l can be found analytically. Their intersection points may not be analytically findable, however, or their expressions may be too complicated to be useful. Even so, graphical solution may be an instructive and intuitive approach to solving the background stability problem.

Returning to the solitons, we note that as g_0 is moved around in the X, Y plane, the number of intersections of N and L can change. When N is tangent to L, there is a saddle-node bifurcation, because any further leftward movement of N (e.g. by reducing the gain $\mathrm{Re}(g_0)$) means that the curves no longer intersect. Of the two soliton solutions created at the saddle-node, at least one must be unstable. Indeed we find that the lower-amplitude soliton is always unstable, and is a separatrix between the no-soliton state and the larger-amplitude soliton. The latter turns out to be stable, at least numerically, over a finite range beginning at the saddle node.

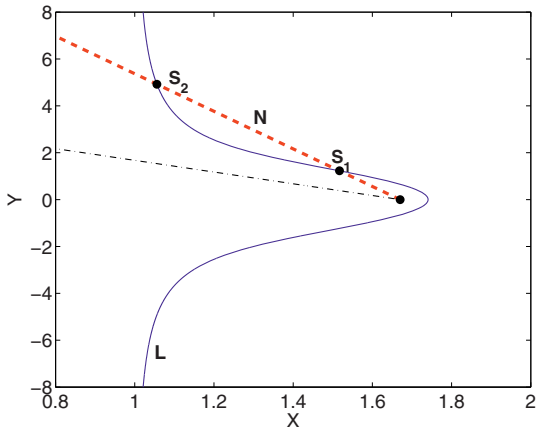

Fig. 3. (Color online) Spectral curve for a weakly-coupled resonant linear loss model, cf. [17]. The soliton line (N) intersects the spectral curve (L) twice, corresponding to two soliton solutions, while the linear-waves line (dash-dotted) does not intersect it, so that the soliton background is stable.

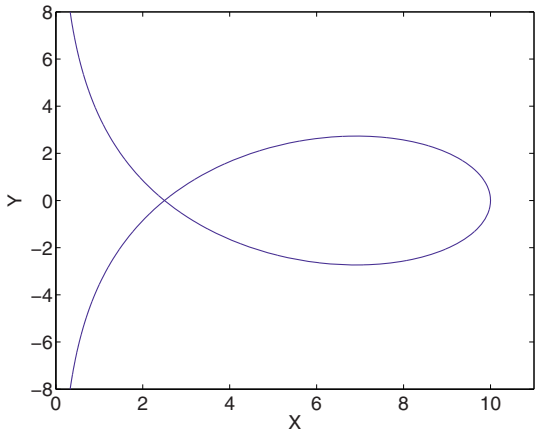

Fig. 4. (Color online) Spectral curve for mode-locked fibre laser model [18].

Chirped-sech solitons, numerically stable over significant parameter ranges, were found over a decade ago in a time-domain model [17]. Atai and Malomed analyzed a fibre-amplifier model describable by the CGL3 (and so with unstable solitons), but coupled to a second fibre with resonant loss. Their model thus corresponds to setting $\sigma < 0$ in (9). As one might expect, for such a case L can be quasi-Lorentzian (Fig. 3), like a "flipped" version of Figure 2. For some parameters, however, L can acquire a loop, which occurs when $dY/d\Omega$ changes sign in the resonant response region (Fig. 4). In between, there is a critical case in which the loop degenerates into a cusp. This occurs for $\sigma = -1$, the case appropriate to the fibre model considered in [17].

In any of these cases, it is clear that the soliton curve emerging from a stable g_0 can intersect L twice only if g_0 lies to the right of L's asymptote, i.e. "inside" L's resonance region, see Figure 3. In turn, this means that $d \neq 0$ is necessary to prevent linear instability: d has to

be large enough that the linear-mode curve N_l does not intersect L, but N does (Fig. 3). In the fibre case, d represents gain linewidth. Mathematically and geometrically, the nonlinear gain g_2 should be such that the soliton line N is steeper than N_l, so that, on increasing the linear gain, N crosses L first. Physically, the short-pulse soliton has a broad enough spectrum to be only weakly affected by the resonant loss, but not so broad that it loses too much gain.

Numerically-stable chirped-sech solitons have been found in this model for both signs of the dispersion (D) [17,33]. While it would be interesting to apply our geometrical approach to the various cases of this coupled-fibre amplifier problem, it would take us into more detail than is appropriate in this paper. Instead, we turn to a second instance of a time-domain problem, this time a mode-locked fibre-laser model.

Kutz and co-workers, in a series of papers [18], see also chapter 10 of [1], consider a fibre laser model in which the output of the amplifying fibre is fed back to its input via an array of resonantly-coupled waveguides. These are arranged so that the fibre output couples into just one member of the array, and only that waveguide feeds back into the fibre. If the injected field is weak, it readily couples across the array, and little is reinjected into the fibre. A large-amplitude field decouples from the other guides because of nonlinearity, so is re-injected more efficiently, and thus sees lower round-trip loss. Loss which reduces for high amplitudes is the standard approach to achieve short-pulse operation, i.e. mode-locking. Our particular interest in this model is due to the fact that these authors find stable pulses of chirped-sech type, which we here interpret as due to curvature of L, rather than N (as in lasers which are mode-locked by introducing a saturable absorber into the cavity).

In [18] the model is simplified by reducing the array to just five elements, and furthermore using symmetry to effectively reduce the number of coupled fields to three, described by equation (5) of the Kutz-Sanstede paper [18]. In terms of our approach, their equations are essentially equivalent to (9), with the addition to $\hat{L}$ of a third field G which obeys

$$\partial_t G + (\Gamma_G + i\Omega_0)\, G = \sigma^{\frac{1}{2}} F. \tag{13}$$

As in [18] we allow G to have different damping from E and F. By symmetry, F must be driven now by both E and G, though in practice E is much stronger. These authors choose parameters such that L takes the form shown in Figure 4. The large coupling coefficient used is the main difference from Figure 3, but the loop in L makes little difference in practice, because the gain point g_0 must again lie to the left of L, but to the right of its asymptote, to achieve a double intersection of L and N (Fig. 4). Again, therefore, finite d (spectral bandwidth) is essential to stabilize the background.

An interesting feature of this model is that $\hat{N}$ is not the basic CGL3 nonlinear operator, but includes gain saturation. The nature of the fibre amplifier is such that gain saturation is global, dependent on the pulse energy, rather than the local intensity. As a result, g_0 can be replaced in $\hat{N}$ by a "fixed-gain" parameter g_f given by [18]:

$$g_f = \frac{e_0 g_0}{e_0 + \int_{-\infty}^{\infty} |E(t')|^2\, dt'}. \tag{14}$$

Here e_0 is a saturation energy. Using g_f in $\hat{N}$ enables N to be found using a chirped-sech pulse *ansatz*, for which the pulse energy is given by $\int_{-\infty}^{\infty} |E(t')|^2 dt' = 2A^2/K$, where A is the soliton's peak amplitude and K its width, as before (except that K now relates to the time domain). One can thus solve the unsaturated-gain problem using g_f, and self-consistently relate it to the physical gain parameter.

Again, to go further into this problem is beyond our present scope. Instead we merely note that it is another example of a separable CGL3 generalization, and take its introduction of global gain saturation as a cue to go beyond CGL3 by considering *local* gain saturation in the next section.

4 Saturable gain models and multi-dimensional dissipative solitons

In the previous section we gave several examples of how a resonant linear coupling can modify the spectral curve so as to produce stable chirped-sech solitons even with cubic nonlinearity. Our last example went beyond the cubic approximation in its treatment of gain saturation, albeit while still admitting chirped-sech solitons. In this section we examine models with local, not global, gain saturation, which is usually the case in the spatial domain. This will enable us to look at forms of $\hat{N}$ which are more realistic for VCSELs than the "toy" version (10). In semiconductor lasers the gain arises from a population inversion of electrons between conduction and valence bands, an inversion which has its own relaxation dynamics. Based on [21,32] we can write a suitable $\hat{N}$ operator:

$$\begin{cases} \hat{N}E = i\nabla^2 E + \Sigma(1 - i\alpha)(n-1)E, \\ \\ \partial_t n = -\gamma \left[n - J + |E|^2 (n-1) + d_e \nabla^2 n \right]. \end{cases} \tag{15}$$

Here we have allowed for two transverse dimensions, and Σ is a field-carrier coupling constant. The electron-hole population is described by n, with dynamics given by the second member of (15): it has relaxation rate γ, is driven by a current density J, is affected by stimulated emission (absorption) when $n > 1$ (<1), and diffuses spatially with strength d_e. (All variables are scaled and dimensionless.)

Note that (15) has no surviving time dependence for equilibrium states in which E is single-frequency, so that electron dynamics, even diffusion, does not invalidate our $\hat{N}$, $\hat{L}$ separation for such states. Of course, we can no longer expect chirped-sech, or indeed any analytic, soliton solutions. Numerical solutions of (15) can be found for a variety of types of self-localized structures, and the resulting N curves can be plotted in the X, Y plane in conjunction with the above spectral curves (or others of interest) to identify solutions of the complete problem.

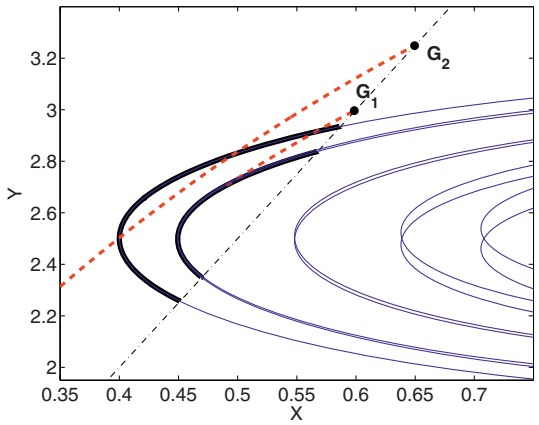

Fig. 5. (Color online) Multiple arcs of the spectral curve for FSF VCSEL with delay (solid thin line) [20]. Varying current with constant spectral parameters, 2D soliton solutions trace out parts (solid bold lines) of the spectral arcs, while varying spectral parameters at constant current the computed soliton solutions trace out the 2D-soliton curve (dashed), here displayed for two different currents.

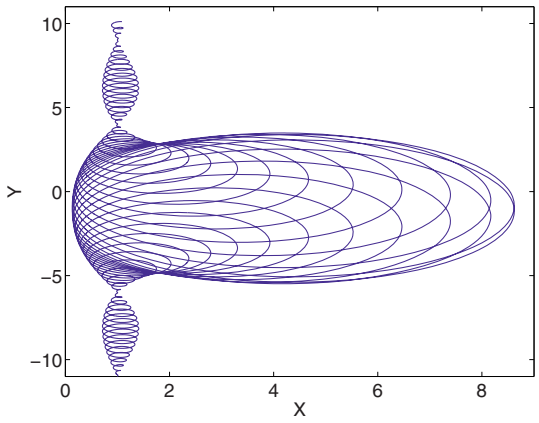

Fig. 6. (Color online) Spectral curve for laser with external grating feedback [21].

It is instructive (and a good approximation in typical VCSEL models [32]) to neglect electron diffusion, in which case we can solve for n, obtaining a reduced nonlinear operator:

$$\hat{N}E = i\nabla^2 E + \Sigma(1 - i\alpha)\frac{J-1}{1+|E|^2}E. \qquad (16)$$

We note that gain saturation here takes the standard saturation denominator form, but is local, i.e. depends on $|E|^2$ rather than its integral over space, as in the fibre-laser case described above. Evidently there is gain if $J > 1$: we can identify $\Sigma(J-1)$ with the gain parameter μ in (10).

Numerical evaluation of the soliton curve for the 1D version of (16) shows it to be somewhat, but not dramatically, curved, with soliton profiles very similar to the CGL3 chirped-sech profile, to which they tend in the small-amplitude limit.

Instead of dwelling on that case, we present 2D soliton results in Figure 5. Here the spectral curve corresponds to (9), but now with finite delay in the feedback. As a consequence, the phase of the feedback parameter σ rotates like $e^{i\Omega\tau_f}$, where τ_f is the feedback delay [20]. L therefore loops back and forward between phases of positive and negative feedback. Only those arcs of highest resonant feedback are shown in Figure 5, in which the data points are obtained by varying parameters in the full partial differential equation [20], illustrating a convenient empirical method of plotting spectral and structure lines. Varying any parameter in $\hat{N}$, such as the current parameter μ, traces out a section or sections of the spectral curve L, while conversely, varying any parameter in $\hat{L}$ traces out the structure curve N. In particular, solving the complex eigenvalue problem $\hat{N}E = (X - iY)E$ is equivalent to finding single-frequency solutions, with frequency Y, of the PDE problem $\hat{N}E = XE + i\partial_t E$. Hence the wide range of analytic, approximate, and numerical methods which have been developed for nonlinear wave equations can be adapted to solve the sort of complex eigenvalue problem under consideration.

Curves for cylindrically-symmetric 2D solitons, obtained by this method, are illustrated in Figure 5 for two different current values. These curves, like the 1D soliton curves, originate on the line $(X = \mu, Y = \mu\alpha)$ which is the locus of the complex linear gain as the current is increased. The curvature of the 2D soliton line is very small in this example, and so the 2D soliton phenomenology is very similar to that of the simple 1D cubic limit already discussed. The upper curve (larger current) intersects the outermost arc of L twice, corresponding to a low-amplitude, broad 2D soliton (upper intersection) and a narrower, larger-amplitude one (lower intersection). Again, the low-amplitude soliton is found to be an unstable separatrix, while the other is stable over a broad range [20,34]. It is evident that a saddle-node will occur if the current is increased a little from G_2 in Figure 5. The side-mode solitons at the lower-current point G_1 are evidently very close to their saddle-node, the soliton curve being almost tangent to that spectral arc.

Were the current to be further reduced from G_2, the limit point of the soliton curve will cross the upper spectral arc, and one solitonic intersection will disappear. In line with our earlier discussion, the remaining soliton should be unstable due to background instability – the linear wave line N_l now intersects L (compare Fig. 2) – and indeed this is is the case.

These 2D soliton curves are somewhat less steep than for 1D. Their slope can be quite accurately estimated perturbatively, based on the 2D "Townes soliton" of the NLS, giving approximately $\alpha/2$, whereas the 1D line has slope close to $3\alpha/4$. Hence the 2D soliton's saddle node is at lower current than for 1D [34].

We briefly re-iterate that these soliton curves can be used with other spectral curves, for example, Figure 6, which shows the spectral curve for the case where feedback is by reflection from a diffraction grating, rather than a filter, and where multiple reflections in the feedback loop are taken into account [21]. The multiple loops

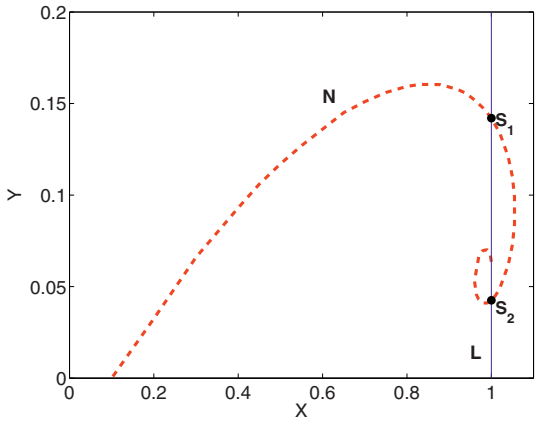

Fig. 7. (Color online) Soliton curve for laser with saturable absorber (Chap. 5 of [1]).

corresponding to external-cavity modes are clearly seen, while their envelope is sinc-like, a signature of the grating response. Such multi-looped spectral curves rather easily give rise to intersections of high multiplicity, even with a half-line soliton curve. Then there is coexistence of multiple soliton solutions corresponding to different longitudinal modes of the feedback system. One can therefore expect noise-induced mode-hopping, which is seen in experiment [10,22]. One can also expect dynamical mode competition [21], though its details are obviously beyond our present geometrical approach.

Lastly in this section, we now examine a simple model of a laser with saturable absorber, whose solitonic properties have been discovered, and extensively discussed by Rosanov and co-workers in [23] and a series of subsequent papers: see chapter 5 of [1]. Recall that the LSA is designed to be bistable, enabling its soliton curve to have two or more intersections, even with the trivial spectral curve given by $L = 1 - i\Omega$. Historically, direct numerical solution has been adopted, but here we apply our separation approach, with a view to consideration of LSA in systems with non-trivial spectral curves.

We choose a very simple form for $\hat{N}$, that used by Rosanov in chapter 5 of [1], for which solitons exist in one, two and three dimensions. The nonlinear operator takes the form

$$\hat{N}E = i\nabla^2 E + \frac{g_0}{1+|E|^2}E - \frac{a}{1+b|E|^2}E. \qquad (17)$$

Following Rosanov in [1], we use $a = 2$ for the linear absorption strength and $b = 10$ for its saturation parameter. Figure 7 shows the 1D soliton curve for gain parameter $g_0 = 2.1$. In the cubic limit of this problem the chirp parameter is $\beta = -\sqrt{2}$, which determines the gradient of the soliton curve close to its origin. As expected, at higher amplitudes the curve bends downward, crossing the trivial spectral line $X = 1$ twice (the second intersection being stable, from previous work, e.g. [1]). It then spirals around, and would eventually reach a limit point which corresponds to the Maxwell equilibrium point between the extended "on" state and the "off" state. The soliton curves for other values of g_0 are similar in shape, and therefore stable solitons can be found only over a fairly narrow range of gain, because the spiraling range, which is quite narrow, will often occur either below or above the line $X = 1$.

One new result that we can deduce from this soliton curve is that the model should give stable solitons rather easily if interfaced to a linear resonant system, with a spectral curve somewhat similar to that in Figure 2. Furthermore, the soliton intersections can be made to occur on the initial stretch of the soliton curve, where the cubic CGL3 approximation to $\hat{N}$ should be sufficient.

Summarizing this section, we have seen that introduction of saturable nonlinearity, while no longer allowing analytic calculation of the soliton curves, does not radically alter the picture derived in the CGL3 limit, even 2D soliton lines turning out to be rather straight and well-behaved. The laser with saturable absorber aligns with the other cases considered if one introduces a non-trivial spectral operator.

We also considered highly non-trivial spectral curves, corresponding to multi-mode feedback systems, within which we could identify the coexistence of solitons belonging to different modes. Noise-induced hopping between such modes is observed in relevant experiments [10,22]. Finally, we noted that parameter variation in one of the separate problems is a convenient way to trace out the complex eigenvalue curve belonging to the other.

5 Conclusion

In this paper we have developed the idea of separability of dissipative soliton equations to give a geometrical picture of how solitons can arise in such equations, how their background stability can be assessed, and how they evolve with parameters. Our approach also shows how results from one problem can be adapted for use in another, possibly quite different, problem. In particular, we have unified several disparate approaches to the stabilization of solitons of the complex Ginzburg-Landau equation with cubic nonlinearity (CGL3). While much of the work presented in this way is a reformulation of previously published work, our cubic approximation to the VCSEL nonlinearity, and hence the existence of exact (and potentially stable) analytic solitons in such systems, has not, to our knowledge, been previously presented.

It seems that coupling almost any resonant linear system to the CGL3 enables soliton stabilization with appropriate parameter choices, such choices being efficiently guided by consideration of the geometry of the corresponding spectral and soliton lines in the complex eigenvalue plane. We also suggest that resonant linear coupling may profitably be applied to known systems where soliton stabilization has, instead, been achieved by invoking higher-order nonlinearity. Indeed, because multimode optical systems necessarily involve resonant modulation of linear losses, we venture to suggest that an unrecognized linear-coupling mechanism of such a kind, rather than higher-order nonlinearity, may underlie some existing observations of optical dissipative solitons.

In this article we have applied the separation technique only to solitons in one and two dimensions, but it can be readily be extended to other kinds and dimensions of nonlinear structure. 3D structures (optical bullets) are an obvious example, though one can also consider "zero-dimension" structures, i.e. homogeneous nonlinear waves, which will normally be in competition with solitons. Among other self-localized structures, multi-humped clusters and, in 2D, vortex solitons are interesting examples. One can also consider dark solitons − indeed any single-frequency nonlinear wave problem ought to be separable and so can be handled in the way which we have described. This would lead naturally to consideration of employing resonant linear coupling as an effective route to robust stabilization of such structures.

A major present limitation of our separation approach is that it cannot directly yield stability information. True, we have inferred stability information from the geometry of the intersections of spectral and soliton curves. Furthermore, the essential property of stability of the soliton background is separable, and so can be analyzed in our framework. However, it is not yet clear how, or even whether, inferences as to the existence of Hopf instabilities (for example) can be drawn from the topology of our spectral and structure curves. It will therefore be interesting to re-analyze soliton stability analysis in terms of $\hat{L}$ and the linearization of $\hat{N}$. It would be surprising indeed if useful stability information can not be gleaned from the geometry of their complex eigenvalue curves.

This work was supported in part by the EU FET Open Project FunFACS. P.V. Paulau acknowledges financial support from MEC (Spain) and FEDER (EU) through project No. FIS2007-60327 FISICOS. We gratefully acknowledge helpful discussions with many FunFACS partner collaborators and colleagues, in particular Andrew Scroggie, Gian-Luca Oppo and Thorsten Ackemann.

References

1. *Dissipative solitons*, Lecture Notes in Physics, edited by N. Akhmediev, A. Ankiewicz (Springer, New York, 2005), Vol. 661
2. *Dissipative solitons: From Optics to Biology and Medicine*, Lecture Notes in Physics, edited by N. Akhmediev, A. Ankiewicz (Springer, New York, 2008), Vol. 751
3. T. Ackemann, W.J. Firth, G.-L. Oppo, Adv. At. Mol. Opt. Phys. **57**, 323 (2009)
4. *Focus Issue on Dissipative Localized Structures in Extended Systems*, edited by M. Tlidi, M. Taki, Chaos **17**, 037101 (2007)
5. L.A. Lugiato, IEEE J. Quantum Electron. **39**, 193 (2003)
6. S. Barland et al., Nature **419**, 699 (2002)
7. V.B. Taranenko, C.O. Weiss, Appl. Phys. B **72**, 893 (2001)
8. S. Barbay et al., Opt. Lett. **31**, 1504 (2006)
9. X. Hachair et al., Phys. Rev. A **72**, 013815 (2005)
10. Y. Tanguy, T. Ackemann, W.J. Firth, R. Jäger, Phys. Rev. Lett. **100**, 013907 (2008)
11. Y. Tanguy, N. Radwell, T. Ackemann, R. Jäger, Phys. Rev. A **78**, 023810 (2008)
12. P. Genevet et al., Phys. Rev. Lett. **101**, 123905 (2008)
13. P. Genevet et al., Phys. Rev. A **79**, 033819 (2009)
14. T. Elsass et al., Appl. Phys. B **98**, 327 (2009)
15. R.P. Davey, N. Langford, A.I. Ferguson, Elect. Lett. **27**, 1257 (1991)
16. A.B. Grudinin, D.J. Richardson, D.N. Payne, Elect. Lett. **28**, 1391 (1992)
17. J. Atai, B. Malomed, Phys. Lett. A **246**, 412 (1998)
18. J.N. Kutz, B. Sandstede, Opt. Express **16**, 636 (2008)
19. F.W. Wise, P. Di Trapani, Opt. Photon. News **13**, 28 (2002)
20. P.V. Paulau, D. Gomila, T. Ackemann, N.A. Loiko, W.J. Firth, Phys. Rev. E **78**, 016212 (2008)
21. A.J. Scroggie, W.J. Firth, G.-L. Oppo, Phys. Rev. A **80**, 013829 (2009)
22. P. Genevet, Ph.D. thesis, Univ. Nice (2009)
23. N.N. Rozanov, S.V. Fedorov, Opt. Spektrosk. **72**, 1394 (1992) [Opt. Spectrosc. **72**, 782 (1992)]
24. I.S. Aranson, L. Kramer, Rev. Mod. Phys. **74**, 99 (2002)
25. L.M. Hocking, K. Stewartson, Proc. Roy. Soc. Lond. A **326**, 289 (1972)
26. N.R. Pereira, L. Stenflo, Phys. Fluids **20**, 1733 (1977)
27. P.A. Bélanger, L. Gagnon, C. Paré, Opt. Lett. **14**, 943 (1989)
28. C. Paré, L. Gagnon, P.A. Bélanger, Opt. Commun. **74**, 228 (1989)
29. N.N. Rosanov, *Spatial hysteresis and optical patterns*, Springer Series in Synergetics (Springer, Berlin, 2002)
30. M. Bache et al., Appl. Phys. B **81**, 913 (2005)
31. N. Radwell, T. Ackemann. IEEE J. Quantum Electron. **45**, 1388 (2009)
32. L. Spinelli et al., Phys. Rev. A **58**, 2542 (1998)
33. B. Malomed, Chaos **17**, 037117 (2007)
34. P.V. Paulau, D. Gomila, P. Colet, M.A. Matías, N.A. Loiko, W.J. Firth, Phys. Rev. A **80**, 023808 (2009)